

Phase structure evolution and its effect on magnetic and mechanical properties of B-doped Sm_2Co_{17}-type magnets with high Fe content

Yao-Wen Li(李耀文), Zhuang Liu(刘壮), Hai-Chen Wu(吴海辰), Fang Wang(王芳), Chao-Qun Zhu(竺超群), Dong-Liang Tan(谭栋梁), Yu Liu(刘宇), Yang Yang(羊杨), Ming-Xiao Zhang(张明晓), Ren-Jie Chen(陈仁杰), and A-Ru Yan(闫阿儒)

Citation: Chin. Phys. B, 2024, 33 (**9**): 097504. DOI: 10.1088/1674-1056/ad5535
Journal homepage: http://cpb.iphy.ac.cn; http://iopscience.iop.org/cpb

What follows is a list of articles you may be interested in

First-principles study of electronic and magnetic properties of Fe atoms on Cu_2N/Cu(100)

Jiale Chen(陈佳乐) and Jun Hu(胡军)
Chin. Phys. B, 2024, 33 (**8**): 087502. DOI: 10.1088/1674-1056/ad5275

Crystal growth, magnetic and electrical transport properties of the kagome magnet RCr_6Ge_6 (R=Gd-Tm)

Xingyu Yang(杨星宇), Qingqi Zeng(曾庆祺), Miao He(何苗), Xitong Xu(许锡童), Haifeng Du(杜海峰), and Zhe Qu(屈哲)
Chin. Phys. B, 2024, 33 (**7**): 077501. DOI: 10.1088/1674-1056/ad3dcf

Analytical solutions to the precession relaxation of magnetization with uniaxial anisotropy

Ze-Nan Zhang(张泽南), Zhen-Lin Jia(贾镇林), and De-Sheng Xue(薛德胜)
Chin. Phys. B, 2024, 33 (**4**): 047502. DOI: 10.1088/1674-1056/ad08a3

Mechanical and magnetocaloric adjustable properties of Fe_3O_4/PET deformed nanoparticle film

Fengguo Fan(范凤国) and Lintong Duan(段林彤)
Chin. Phys. B, 2024, 33 (**3**): 037502. DOI: 10.1088/1674-1056/acf280

Creation and annihilation of artificial magnetic skyrmions with the electric field

Jun Cheng(程军), Liang Sun(孙亮), Yike Zhang(张一可), Tongzhou Ji(吉同舟), Rongxing Cao(曹荣幸), Bingfeng Miao(缪冰锋), Yonggang Zhao(赵永刚), and Haifeng Ding(丁海峰)
Chin. Phys. B, 2024, 33 (**3**): 037501. DOI: 10.1088/1674-1056/ad188f

---

Phase structure evolution and its effect on magnetic and mechanical properties of B-doped Sm_2Co_{17}-type magnets with high Fe content

Yao-Wen Li(李耀文)[1,2], Zhuang Liu(刘壮)[2,3,†], Hai-Chen Wu(吴海辰)[2], Fang Wang(王芳)[1,‡], Chao-Qun Zhu(竺超群)[2], Dong-Liang Tan(谭栋梁)[2], Yu Liu(刘宇)[2], Yang Yang(羊杨)[2], Ming-Xiao Zhang(张明晓)[2,3], Ren-Jie Chen(陈仁杰)[2,3], and A-Ru Yan(闫阿儒)[2,3]

[1] *Key Laboratory of Magnetic Molecules and Magnetic Information Materials of Ministry of Education & School of Chemistry and Materials Science, Shanxi Normal University, Taiyuan* 030032, *China*

[2] *CISRI & NIMTE Joint Innovation Center for Rare Earth Permanent Magnets, Ningbo Institute of Material Technology and Engineering, Chinese Academy of Sciences, Ningbo* 315201, *China*

[3] *University of Chinese Academy of Sciences, Beijing* 100049, *China*

(Received 5 March 2024; revised manuscript received 24 May 2024; accepted manuscript online 7 June 2024)

The unique cellular microstructure of Fe-rich Sm_2Co_{17}-type permanent magnets is closely associated with the structure of the solid solution precursor. We investigate the phase structure, magnetic properties, and mechanical behavior of B-doped Sm_2Co_{17}-type magnets with high Fe content. The doped B atoms can diffuse into the interstitial vacancy, resulting in lattice expansion and promote the homogenization of the phase organizational structure during the solid solution treatment in theory. However, the resulting second phase plays a dominant role to result in more microtwin structures and highly ordered 2 : 17R phases in the solid solution stage, which inhibits the ordering transformation of 1 : 7H phase during aging and affects the generation of the cellular structure, and to result in a decrease in magnetic properties, yet the interface formed between it and the matrix phase hinders the movement of dislocations and enhances the mechanical properties. Hence, the precipitation of high flexural strain grain boundary phase induced by B element doping is also a new and effective way to improve the flexural strain of Sm_2Co_{17}-type magnets. Our study provides a new understanding of the phase structure evolution and its effect on the magnetic and mechanical properties of Sm_2Co_{17}-type magnets with high Fe content.

Keywords: Sm_2Co_{17}-type magnets, magnetic and mechanical properties

PACS: 75.30.Gw, 68.60.Dv, 71.20.Eh, 75.50.Ww **DOI:** 10.1088/1674-1056/ad5535

1. Introduction

Sm_2Co_{17}-type magnets are extensively utilized in aerospace, microwave devices, high-performance traction motors, and other cutting-edge fields due to their exceptional high-temperature magnetic properties, elevated Curie temperature, remarkable thermal stability, as well as excellent corrosion and oxidation resistance.[1–5] With the ongoing trend towards miniaturization, lightweight design, and enhanced efficiency of advanced devices, the demand for magnetic energy products from Sm_2Co_{17}-type magnets is continuously escalating.[6] The research findings by Ray and Strnat[7,8] have demonstrated that the saturation magnetization and theoretical magnetic energy product of $Sm_2(Co_{1-x}Fe_x)_{17}$ compounds exhibit a rapid increase with rising Fe content. Consequently, Sm_2Co_{17}-type magnets containing higher Fe content serve as an outstanding medium to further enhance the magnetic energy product of Sm_2Co_{17}-type magnets.[9–14] However, the complex crystal structure of the main phase, magnetic crystal anisotropy, and powder metallurgy sintering process during preparation result in poor plastic flexural strain for Sm_2Co_{17}-type magnets. This severely restricts their potential applications' expansion. Since both the magnetic and mechanical properties mutually influence each other for these magnets, improving their mechanical properties while maintaining favorable magnetic characteristics becomes an urgent issue. The nano-cellular structure of Sm_2Co_{17}-type magnets plays a pivotal role in determining their magnetic properties, while the formation of a robust ductile phase within the matrix often impedes the uniform precipitation of this cellular structure, thereby hindering simultaneous enhancements in both mechanical and magnetic properties. Given that the cellular structure is derived from the solid solution precursor, a comprehensive understanding and effective regulation of this precursor will be pivotal in enhancing both magnetic and mechanical properties.

It is widely accepted that the solid solution precursors are mainly composed of phases of 1 : 7H.[15,16] However, recent findings have revealed the intricate nature of the solid solution precursor's structure. In addition to the presence of 1 : 7H, a significant number of ordered micro-domains containing 2 : 17R and 2 : 17H structural units, and their variants have also been observed. Wu *et al.*[13] identified the phase composition of the solid solution as being composed of a polymorphic variant consisting of 1 : 7H + 2 : 17H + 2 : 17R structures

†Corresponding author. E-mail: zliu@nimte.ac.cn
‡Corresponding author. E-mail: wangfanghc@sxnu.edu.cn

© 2024 Chinese Physical Society and IOP Publishing Ltd

through analysis by utilizing characteristic weak spots and short-range ordering microzones diffusely distributed within the disordered matrix of 1 : 7H phase. Ma *et al.*[17] discovered that incomplete migration of dislocations and insufficient diffusion led to formation of an intermediate phase known as 2 : 17R′ during the solid solution stage, which was found to be unfavorable for enhancing magnet coercivity. Jiang *et al.*[18] determined that an increase in Fe content promoted microtwin structure formation within the precursor material with a composition ratio of 1 : 7H, resulting in reduced dislocation density and increased occurrence rates for both 2 : 17R′ and grain boundary phases. Fang *et al.*[19] conducted research indicating that at suitable solid solution temperatures, pure-phase occurrences were limited to only having a composition ratio of 1 : 7H. However, higher or lower treatment temperatures would result in occurrences involving both 2 : 17H and even lower ratios such as those seen in compositions like the aforementioned.

To optimize the solid solution structure, various strategies have been explored. Recently, Zhang *et al.*[20] demonstrated that adjusting the Sm content can partially alleviate the occupational competition between Sm/Fe/Zr atoms, thereby stabilizing the 1 : 7H phase. Horiuchi *et al.*[21] achieved stabilization of the 1 : 7H phase through a stepped solid solution process and prolonged treatment. Furthermore, deliberate placement of interstitial atoms in the matrix phase significantly influences the degree of ordering in this phase and subsequently affects the formation of the 1 : 7H phase. Raja *et al.*[22] discovered that doping with B-elements enhances the stability of the 1 : 7H phase structure in rapidly quenched samarium cobalt materials, suggesting that B doping that leads to atomic diffusion into the interstitial vacancies could be an effective approach to enhance the stability of 1 : 7H main phase in the solid solution precursor of sintered Sm_2Co_{17}-type magnets. Additionally, B-element doping is employed to induce phases conducive to improve mechanical properties.

In this paper, the phase structure, magnetic properties, and mechanical behavior of B-doped Sm_2Co_{17}-type magnets with high Fe content are investigated. The impact of B element doping on the solid solution's phase structure is analyzed. Furthermore, a detailed discussion on the evolution of the phase structure and its correlation with magnetic and mechanical properties is presented.

2. Experiment

The $Sm(Co_{0.606}Fe_{0.310}Cu_{0.064}Zr_{0.020})_{7.9}B_x$ ($x = 0$, 0.01, 0.02) ingots were obtained through vacuum induction melting process. The ingots were subsequently crushed and jet-milled to powders with an average particle size of approximately 3.4 μm. The powders were then aligned and pressed in a magnetic field strength of 2.0 T, followed by compaction using cold isostatic pressing under a pressure of 160 MPa. The green compacts underwent sintering in argon at temperatures ranging from 1190 ℃ to 1200 ℃ for a duration of 1.5 h. Afterwards, the compacts underwent solid solution treatment at a temperature of 1140 ℃ for a period of six hours before being rapidly cooled to room temperature. The solution-treated magnets were subjected to isothermal aging at a temperature of 830 ℃ for twelve hours, followed by slow cooling down to a temperature of 400 ℃ at a rate of 0.7 K/min and holding for three hours at that temperature. Finally, rapid cooling was conducted until reaching room temperature.

A Talos (TEM-F200X) transmission electron microscope, manufactured by Thermo Fisher, was employed for the structural and compositional characterization. The microscope operated at an accelerating voltage of 200 kV and offered a point resolution of 0.25 nm. Additionally, it featured a scanning transmission mode with a point resolution of 0.16 nm and was equipped with a four-probe energy spectrum for analysis. The elemental distribution and grain size of the microstructure were analyzed using an electron probe x-ray micro-analyzer (EPMA, JEOL, JXA-ihp200F). To examine the phase structure of the solid solution precursor sample, x-ray diffraction (XRD, Bruker D8 Advance Davinci) with Cu K_α radiation was utilized. Mechanical properties were evaluated using a 30 KN (Zwick/Roell Z030) universal material testing machine ($h \times b \times l = 5$ mm $\times$ 6 mm $\times$ 20 mm), while magnetic properties were measured employing a pulsed field magnetometer (PFM14.CN).

3. Results and discussion

3.1. Phase composition

The primary function of solid solution treatment is to disrupt the high-order structure formed during sintering and homogenize the phase structure of the solid solution. We conducted a microstructural analysis on solid solution treated magnets, as depicted in Fig. 1, which presents EPMA SEM images for the $Sm(Co_{0.606}Fe_{0.310}Cu_{0.064}Zr_{0.020})_{7.9}B_x$ ($x = 0$, 0.01, 0.02) solid solution precursor samples. Based on element distribution, three distinct phases were observed: a dark matrix phase, a white Sm_2O_3 phase, and a gray phase distributed along grain boundaries. The components of the matrix phase exhibited uniform distribution throughout all samples examined. In B-free magnets, both matrix and Sm_2O_3 phases were present; however, upon introduction of B doping elements, an abundance of the SmCu-rich phase (indicated by yellow dashed lines) was formed at grain boundaries in addition to the matrix and Sm_2O_3 phases observed previously. Furthermore, it was noted that with increasing levels of B doping elements, in the solid solution magnet, Fe and Co elements are deficient in grain boundary phase, and Sm and Cu elements are enriched here. Analyses by XRD and EPMA mapping indicate that this phase is SmCu-rich.

Table 1. Rietveld analysis results of magnet $Sm(Co_{0.606}Fe_{0.310}Cu_{0.064}Zr_{0.020})_{7.9}B_x$ ($x = 0$, 0.01, 0.02).

Magnets	Phase information of the 1 : 7H phase			Phase information of the 2 : 17R phase		
	a (Å)	c (Å)	Volume fraction (%)	a (Å)	c (Å)	Volume fraction (%)
$x = 0$	4.898	4.110	60.13	8.486	12.334	23.55
$x = 0.01$	4.903	4.113	46.21	8.501	12.339	35.18
$x = 0.02$	4.907	4.115	30.45	8.511	12.343	43.57

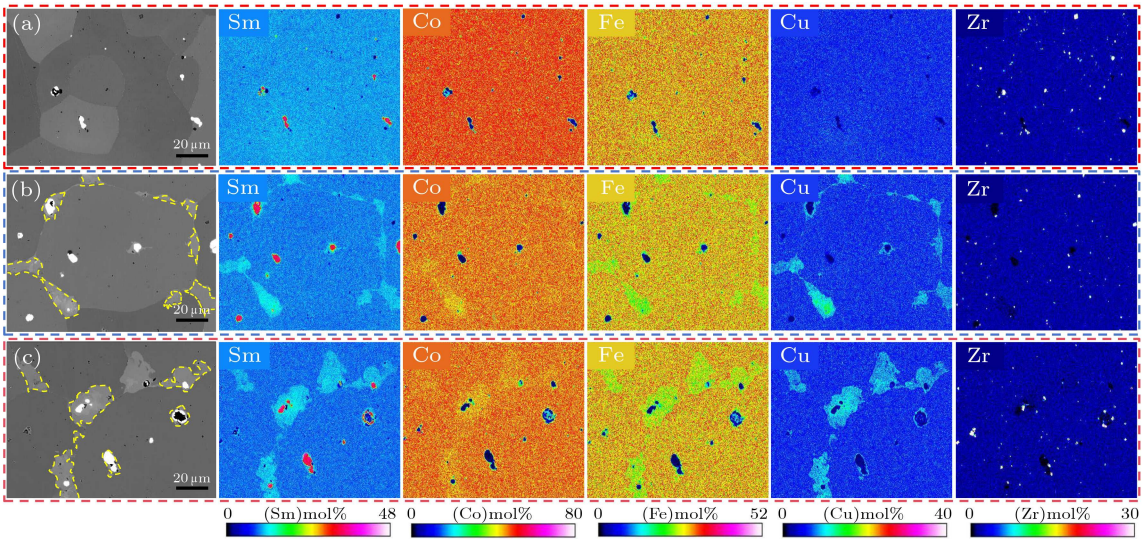


Fig. 1. The EPMA SEM images for the solid solution phase of the magnet $Sm(Co_{0.606}Fe_{0.310}Cu_{0.064}Zr_{0.020})_{7.9}B_x$: (a) $x = 0$, (b) $x = 0.01$, (c) $x = 0.02$.

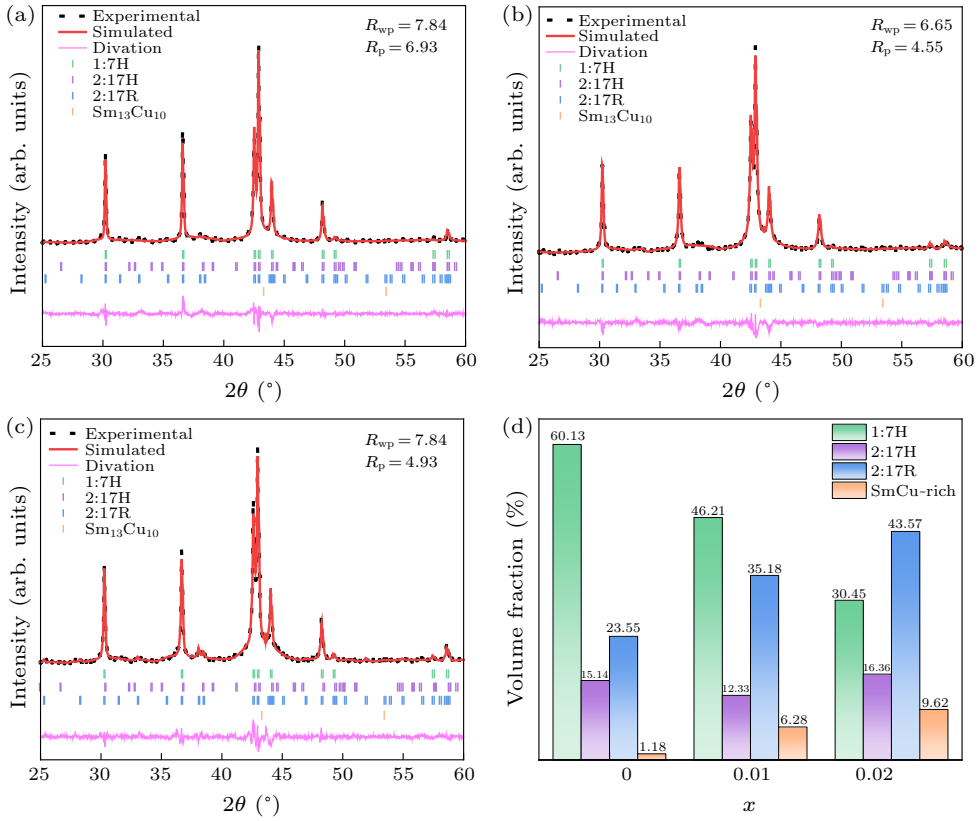


Fig. 2. XRD patterns and refinement results correspond to the solid solution stage magnets $Sm(Co_{0.606}Fe_{0.310}Cu_{0.064}Zr_{0.020})_{7.9}B_x$: (a) $x = 0$, (b) $x = 0.01$, (c) $x = 0.02$. (d) Percentage of the volume fraction depending on x for the solid solution phases. The SmCu-rich phase belongs to the cubic crystal system with the space group of $pm\bar{3}m$(221).

The XRD patterns of solid solution treated Sm_2Co_{17}-type magnets with high Fe content were analyzed to determine their phase composition structure. The refined parameters confirm that our results are acceptable. Table 1 presents phase information obtained from refined analysis of data. With B doping from 0 to 0.2, the lattice constants a and c of the 1 : 7H phase increase from 4.898 Å and 4.110 Å to 4.907 Å and 4.115 Å, respectively, and those of the 2 : 17R phase increase from 8.486 Å and 12.334 Å to 8.511 Å and 12.343 Å, respectively. B atoms doping can stretch the 1 : 7H main phase lattice, reduce the stability of the 1 : 7H phase, lead to the generation and precipitation of heterophase, and inhibit the generation of homogenized phase structures in the solid solution stage.

According to the XRD peaks and fitting results, the matrix phases of the solid-solution magnets exclusively consist of 2 : 17R, 1 : 7H, 2 : 17H and SmCu-rich phases. Figure 2(d) illustrates the volume fraction of each phase in different B-doped magnets. The findings demonstrate that with an increase in B doping content, there is a gradual decrease in the content of the 1 : 7H phase accompanied by an increase in the content of the 2 : 17R and SmCu-rich phase, while the ratio of the 2 : 17H phase remains relatively unchanged. These results indicate that element B doping impedes precipitation of the 1 : 7H phase and enhances formation of the ordered 2 : 17R phase. Furthermore, minimal variation in corresponding diffraction angles suggests limited effective dissolution of element B into dominant phases based on consistent superimposition observed from peak positions.

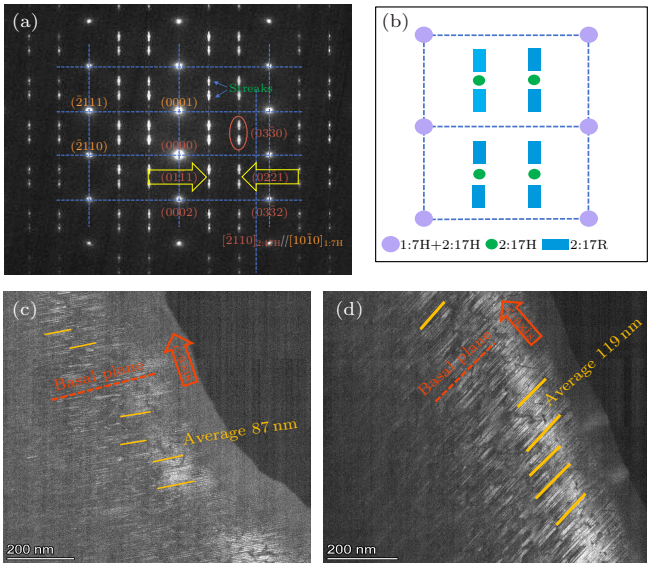


Fig. 3. (a) TEM images with SAED patterns of the original solution sample. (b) Schematic SAED patterns of the solution sample. [(c), (d)] The solid solution dark field images of magnets $Sm(Co_{0.606}Fe_{0.310}Cu_{0.064}Zr_{0.020})_{7.9}B_x$ for (c) $x = 0$ and (d) $x = 0.02$.

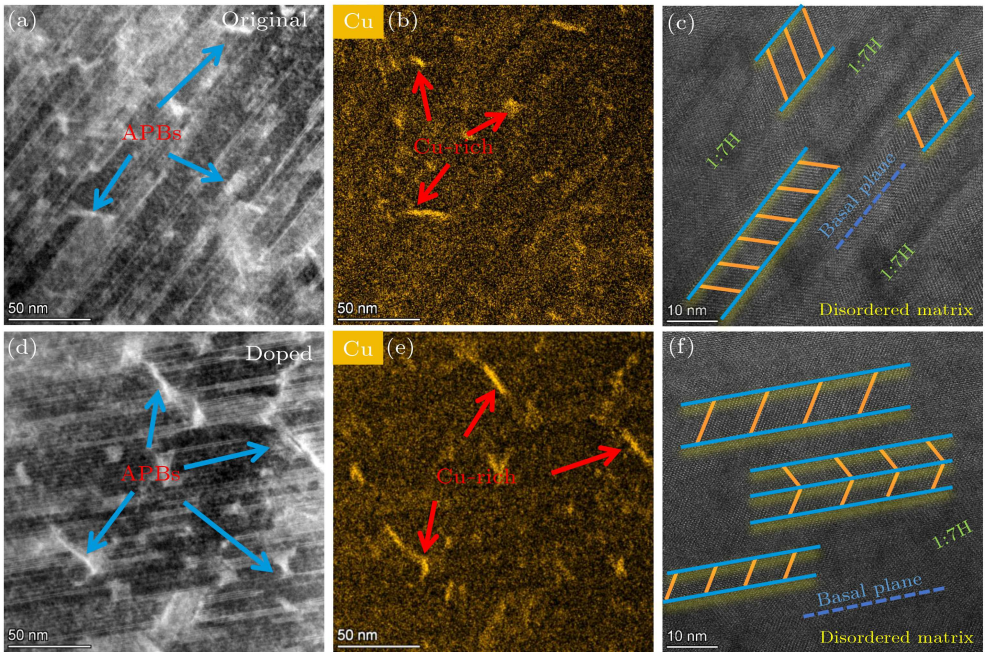


Fig. 4. High-resolution STEM-BF images of the solution-treated magnets: (a) $x = 0$, (d) $x = 0.02$. [(b), (e)] Elemental mapping of Cu in the sample corresponding to (a) and (d). [(c), (f)] The HRTEM images of the solution-treated magnets for (c) $x = 0$ and (f) $x = 0.02$.

3.2. Microstructures of the solution-treated magnets

The TEM images in Fig. 3(a) display SAED patterns of the solution sample along the $\langle 10\bar{1}0\rangle_{1:7H}$ zone axis. The characteristic diffraction spots of 2 : 17H, located at $(01\bar{1}1)$ and $(02\bar{2}1)$, are not clearly discernible. However, the distinct streaks along the (000l) direction appear at the position where superlattice diffraction spots occur for the 2 : 17R twin variants. Schematic SAED patterns of the solution sample

along both the common $\langle 10\bar{1}0\rangle_{1:7H}$ and $\langle 2\bar{1}10\rangle_{2:17H}$ zone axes are presented in Fig. 3(b). Further analysis revealed minimal changes in the SAED pattern depicted in Fig. 3(a) during solid solution treatment of doped samples, indicating an almost unchanged phase structure but significant alterations in phase content as confirmed by refined XRD measurements. Dark field images captured using elongated stripes from the 1 : 7H + 2 : 17H + 2 : 17 polymorphic variant are displayed in Figs. 3(c) and 3(d), representing initial magnet and doped samples, respectively. In Fig. 3(c), a high density and regular arrangement of stripes can be observed along the basal plane with a measured length of approximately 87 nm; whereas after B doping as shown in Fig. 3(d), stripe length increases to around 119 nm, signifying an enhanced degree of ordered micro-regions.

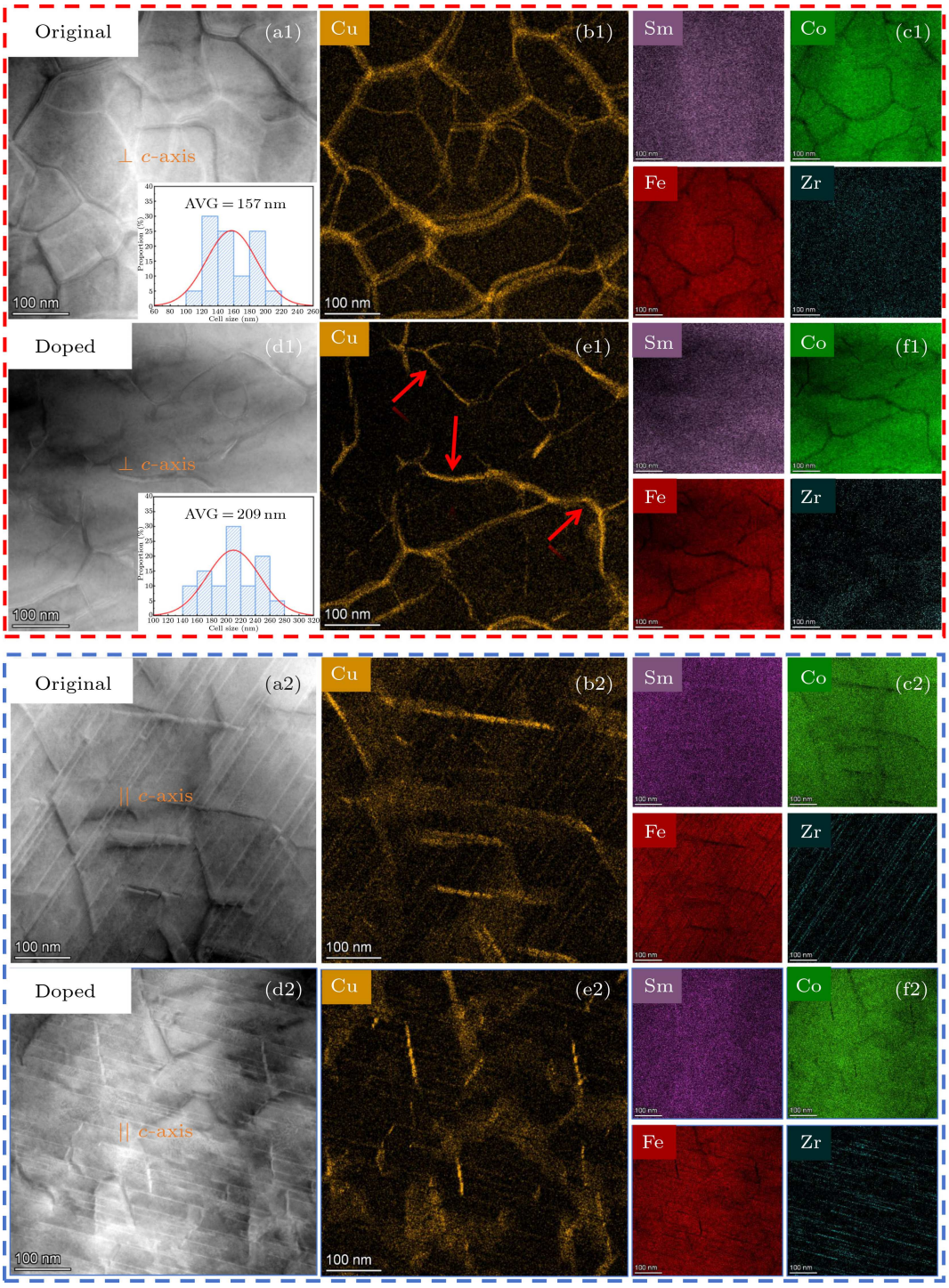


Fig. 5. The aging treated magnets are perpendicular and parallel to the c-axis, respectively. [(a1), (a2), (d1), (d2)] HADDF images for [(a1), (a2)] $x = 0$ and [(d1), (d2)] $x = 0.02$. [(b1), (b2), (e1), (e2)] EDS mappings of Cu. [(c1), (c2), (f1), (f2)] EDS mappings of Sm, Co, Fe, and Zr in magnets $Sm(Co_{0.606}Fe_{0.310}Cu_{0.064}Zr_{0.020})_{7.9}B_x$. The red arrows indicate the narrow Cu-rich regions.

The high-resolution STEM-BF images of the solution-treated magnets with $x = 0$ and 0.02 are presented in Fig. 4, accompanied by the corresponding Cu elemental mapping. Figures 4(a) and 4(d) reveal a distinct striped structure and the presence of white defects in all solution-treated magnets. In terms of elemental distribution, the white defect regions exhibit an enrichment of copper, with even distribution within the ordered microregions. Based on previous research findings,[16] these white defect regions correspond to antiphase domain boundaries between adjacent ordered microdomains along the basal plane direction. As depicted in Figs. 4(b) and 4(e), a higher density of Cu-rich antiphase domain boundaries is observed at the interruption point of the nanotwin structure along the direction parallel to the basal plane before and after B doping. Simultaneously, HRTEM analyses Figs. 4(c) and 4(f) reveal a decrease in the percentage of 1 : 7H phase content and an increase in ordering degree. In magnets with high Fe content, an increasing number of antiphase boundaries (APBs) are formed after B doping compared to initial magnets.

3.3. Microstructures of the final magnets

The cellular structure of Sm_2Co_{17}-type magnets, as a representative precipitation-hardened magnet, plays a crucial role in determining their magnetic properties. Figure 5 presents the high-angle annular dark field (HAADF) image and energy-dispersive x-ray spectroscopy (EDS) analysis of aged magnets with $x = 0$ and 0.02 oriented perpendicular and parallel to the c-axis, illustrating the transition from a complete and uniform cellular structure to an incomplete cellular structure after B doping, with the average cell size increasing from 157 nm to 209 nm. Besides the cellular structure, the distribution of elements also significantly impacts the performance of Sm_2Co_{17}-type magnets. Specifically, Cu enrichment is observed in the cell wall phase while Zr enrichment occurs in the laminar phase; Co and Fe are enriched within the cellular phase, whereas Sm enrichment is less pronounced. The narrowing of cell boundary phases promotes Cu segregation, resulting in an increase of Cu content from 30.68% to 42.41%. However, this leads to discontinuity and reduction of the width of cell boundary phases from 16.36 nm to 10.62 nm in B-doped magnets, as indicated by red arrows in Fig. 5(e1). Although increasing copper content within certain areas of cell wall phases contributes to improved coercivity, overall discontinuous distribution hinders attainment of superior magnetic properties.

The presence of the SmCu-rich phase can be observed in the aged magnet, as shown in Fig. 6, with the fracture photos given. In the magnet without B atom doping, the cleavage surface at the fracture morphology is smooth and the cleavage step is wider. In the magnet with B atom doping, a large number of fine cleavage steps and stream-like streaks appear at the fracture morphology, and the crack propagation to the fine dissociation step encounters greater resistance, which can effectively improve its mechanical properties.

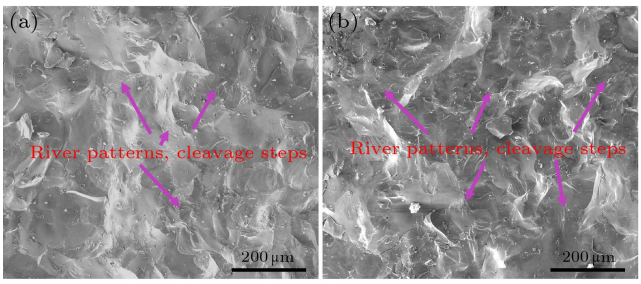


Fig. 6. The SEM images of the fracture surface of $Sm(Co_{0.606}Fe_{0.310}Cu_{0.064}Zr_{0.020})_{7.9}B_x$ aging state magnets: (a) $x = 0$, (b) $x = 0.02$.

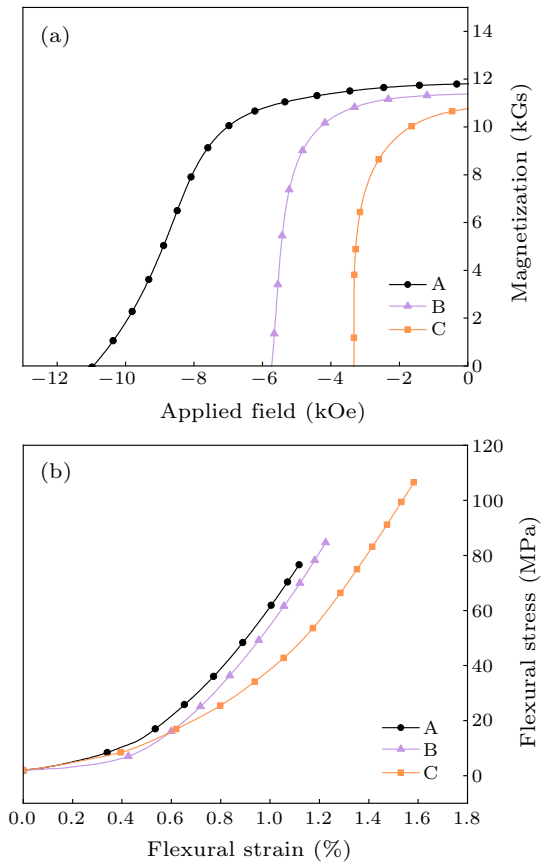


Fig. 7. (a) Room-temperature magnetic properties of magnets A, B, and C. (b) Mechanical properties of magnets A, B, and C.

3.4. Magnetic and mechanical properties

The demagnetization curves of $Sm(Co_{0.606}Fe_{0.310}Cu_{0.064}Zr_{0.020})_{7.9}B_x$ ($x = 0$, 0.01, 0.02) aged magnets (designated as magnets A, B, and C) at room temperature are presented in Fig. 7(a). Magnet A with high Fe content exhibits an intrinsic coercivity H_{cj} of 10.94 kOe and a maximum energy product $(BH)_{max}$ of 30.77 MGOe; both magnets B and C show reduced levels of H_{cj} and $(BH)_{max}$ to varying degrees compared to magnet A. However, the mechanical properties of the magnets exhibited a significant enhancement, with a notable 41% increase in flexural strain from approximately 1.13

to 1.60 and a substantial 39% increase in flexural stress from around 76 MPa to 106 MPa, as illustrated in Fig. 7(b). The enhanced bending stress is attributed to the formation of the SmCu-rich grain boundary phase, which acts as an interfacial reinforcement by hindering dislocation movement and slip while absorbing stress, effectively preventing crack expansion along with hardness improvement leading to increasing material resistance to plastic flexural strain. Doping with element B reduces the solid solution ratio of 1 : 7H along with discontinuous distribution within cell wall phases resulting in decreasing coercivity.

4. Conclusions

We have provided a comprehensive investigation on evolution of phase structure and its impact on the magnetic and mechanical properties of B-doped Sm_2Co_{17}-type magnets with high Fe content. The findings demonstrate that the addition of the B element partially supports the lattice, facilitating homogenization of the solid solution phase structure. However, it is observed that heterogeneous phases play a dominant role in microstructure organization. Notably, B-doped magnets exhibit an increasing presence of anti-phase boundaries and significantly elevated 2 : 17R phase content, which enhances the ordering of the solid solution precursor phase. Moreover, while the introduction of a second phase strengthens interfacial bonding and promotes mechanical properties, it also leads to improved magnet flexural strain through high-flexural strain grain boundary phase precipitation induced by B element.

Acknowledgments

This work was financially supported by the National Key R&D Program of China (Grant Nos. 2021YFB3503102 and 2022YFB3505301), Science and Technology Innovation 2025 Major Project of Ningbo (Grant No. 2022Z204), Zhejiang Provincial Natural Science Foundation Youth Original Project (Grant No. LDQ24E010001), the Key R&D Program of Shanxi Province (Grant No. 202302050201014), and Ningbo Natural Science Foundation (Grant No. 2021J216).

References

[1] Ojima T, Tomizawa S, Yoneyama T and Hori T 1977 *Jpn. J. Appl. Phys.* **16** 671
[2] Xiong X Y, Ohkubo T, Koyama T, Ohashi K, Tawara Y and Hono K 2004 *Acta Mater.* **52** 737
[3] Sepehri-Amin H, Thielsch J, Fischbacher J, Ohkubo T, Schrefl T, Gutfleisch O and Hono K 2017 *Acta Mater.* **126** 1
[4] Horiuchi Y, Hagiwara M, Okamoto K, Kobayashi T, Endo M, Kobayashi T, Sanada N and Sakurada S 2014 *Mater. Trans.* **55** 482
[5] Xia W, He Y K, Huang H B, Wang H, Shi X M, Zhang T L, Liu J H, Stamenov P, Chen L Q, Michael J and Jiang C B 2019 *Adv. Funct. Mater.* **29** 1900690
[6] Gutfleisch O, Willard M, Brück E, Chen C, Sankar S and Liu J 2011 *Adv. Mater.* **23** 821
[7] Strnat K 1972 *IEEE Trans. Magn.* **8** 511
[8] Ray A and Strnat K 1972 *IEEE Trans. Magn.* **8** 516
[9] Yu N J, Gao W Y, Pan M X, Yang H F, Wu Q, Zhang P Y and Ge H L 2020 *J. Alloys Compd.* **818** 152908
[10] Hu M Y, Kang D Z, Zhang T L, Liu B J, Xi L L, Cao J, Xu C, Zuo S L, He Y K and Jiang C B 2023 *J. Alloys Compd.* **945** 169373
[11] Wang S, Fang Y K, Wang C, Wang L, Zhu M G and Li W 2020 *J. Magn. Magn. Mater.* **510** 166942
[12] Cao J, Zhang T L, Xu H, Liu J H, Hu M Y and Xi L L, Wang H and Jiang C B 2022 *Scr. Mater.* **209** 114418
[13] Wu H C, Liu Z, Zhang C Y, Yang Q Q, Lu H M, Chen G X, Wang X M, Li Y, Chen R J and Yan A R 2022 *J. Rare Earth.* **40** 102
[14] Wang S, Chen H S, Fang Y K, Wang C, Wang L, Zhu M G and Li W 2021 *Rare Met.* **40** 3567
[15] Wang C, Shen P, Fang Y K, Wang S, Li Q F, Wang L, Li W and Zhu M G 2022 *J. Mater. Sci. Technol.* **120** 8
[16] Wu H C, Zhang C Y, Liu Z, Wang G Q, Lu H M, Chen G X, Li Y, Chen R J and Yan A R 2020 *Acta Mater.* **200** 883
[17] Song X, Ma T Y, Zhou X L, Ye F, Yuan T, Wang J D, Yue M, Liu F and Ren X B 2021 *Acta Mater.* **202** 290
[18] Hu M Y, Yang L, Xi L L, Kang D Z, Zhang T L, He Y K and Jiang C B 2023 *Acta Mater.* **261** 119363
[19] Wang C, Shen P, Fang Y K, Wang S, Li Q F, Wang L, Li W and Zhu M G 2022 *J. Mater. Sci. Technol.* **120** 8
[20] Zhang C Y, Liu Z, Li M, Liu L, Li T Y, Chen R J, Lee D and Yan A R 2018 *Sci. Rep.* **8** 9103
[21] Horiuchi Y, Hagiwara M, Endo M, Sanada N and Sakurada S 2015 *J. Appl. Phys.* **117** 17
[22] Sun J B, Javed A, Zhang Z X, Cui C X, Zhang M X and Han R P 2010 *Mater. Sci. Eng. B* **167** 102